Kinetic Mechanism of the Enantioselective Conversion of Styrene Oxide by Epoxide Hydrolase from *Agrobacterium radiobacter* AD1

Rick Rink and Dick B. Janssen*

Department of Biochemistry, Groningen Biomolecular Sciences and Biotechnology Institute, University of Groningen, Nijenborgh 4, 9747 AG, Groningen, The Netherlands

Received July 17, 1998; Revised Manuscript Received October 14, 1998

ABSTRACT: Epoxide hydrolase from *Agrobacterium radiobacter* AD1 catalyzes the enantioselective hydrolysis of styrene oxide with an *E* value of 16. The (*R*)-enantiomer of styrene oxide is first converted with a k_{cat} of 3.8 s^{-1}, and the conversion of the (*S*)-enantiomer is inhibited. The latter is subsequently hydrolyzed with a k_{cat} of 10.5 s^{-1}. The pre-steady-state kinetic parameters were determined for both enantiomers with stopped-flow fluorescence and rapid-quench techniques. For (*R*)-styrene oxide a four-step mechanism was needed to describe the data. It involved the formation of a Michaelis complex that is in rapid equilibrium with free enzyme and substrate, followed by rapid and reversible alkylation of the enzyme. A unimolecular isomerization of the alkylated enzyme precedes the hydrolysis of the covalent intermediate, which could be observed due to an enhancement of the intrinsic protein fluorescence during this step. The conversion of (*S*)-styrene oxide could be described by a three-step mechanism, which also involved reversible and rapid formation of an ester intermediate from a Michaelis complex and its subsequent slow hydrolysis as the rate-limiting step. The unimolecular isomerization step has not been observed for rat microsomal epoxide hydrolase, for which a kinetic mechanism was recently established [Tzeng, H.-F., Laughlin, L. T., Lin, S., and Armstrong, R. N. (1996) *J. Am. Chem. Soc. 118*, 9436−9437]. For both enantiomers of styrene oxide, the K_m value was much lower than the substrate binding constant K_S due to extensive accumulation of the covalent intermediate. The enantioselectivity was more pronounced in the alkylation rates than in the rate-limiting hydrolysis steps. The combined reaction schemes for (*R*)- and (*S*)-styrene oxide gave an accurate description of the epoxide hydrolase catalyzed kinetic resolution of racemic styrene oxide.

Epoxide hydrolases can convert epoxides to their corresponding diols by the addition of a water molecule without the use of a cofacter. About fifteen epoxide hydrolase genes have been isolated from different organisms, including mammals, insects, plants, fungi, and bacteria. All of the enzymes appear to be structurally and mechanistically similar, including two recently cloned bacterial epoxide hydrolases that are related to the ones cloned from higher organisms (*1*−*4*). The main incentive for studying these enzymes is their key role in the detoxification of xenobiotic compounds in the liver, but increasing attention is given to their great potential in biocatalysis. Epoxide hydrolases from eukaryotic and prokaryotic sources were found to be applicable for the kinetic resolution of racemic mixtures of epoxides, and high enantiomeric excesses have been reported (*5*−*7*). Most detailed studies have been performed on microsomal and soluble epoxide hydrolases from mammalian origin. These include substrate and inhibitor studies, site-directed mutagenesis studies on catalytic residues, and a recently performed pre-steady-state kinetic analysis with rat microsomal epoxide hydrolase (*8*−*10*).

Epoxide hydrolases are classified as α/β-hydrolase fold enzymes (*2*, *11*). The topology of this class of enzymes shows two domains, a main domain that consists of a central β-sheet surrounded by α-helices with the catalytic residues excursing on top of the sheet at loops, and a cap domain that consists predominantly of α-helices and is involved in substrate binding. The mammalian epoxide hydrolases contain an additional N-terminal domain, which has sequence similarity to another class of hydrolytic enzymes in the case of the soluble epoxide hydrolase (*12*), and a membrane anchor involved in bile acid transport in the case of microsomal epoxide hydrolase (*13*). The bacterial epoxide hydrolases cloned up to now are simpler enzymes, since they do not contain these extra N-terminal domains (*3*, *4*). However, they have not yet been studied in great detail.

The epichlorohydrin epoxide hydrolase (EchA)[1] that was used for this study was isolated from *Agrobacterium radiobacter* AD1, a bacterium that is able to grow on epichlorohydrin as the sole source of carbon and energy. The corresponding gene was overexpressed in *Escherichia coli* BL21(DE3) (*4*, *14*). The epoxide hydrolase is a 34 kDa monomeric enzyme that has a broad substrate range. On the basis of the sequence analysis and the behavior of site-

* To whom correspondence should be addressed: Department of Biochemistry, University of Groningen, Nijenborgh 4, 9747 AG, Groningen, The Netherlands. Tel: 31-50-3634209. Fax: 31-50-3634165. E-mail: d.b.janssen@chem.rug.nl.

[1] Abbreviation: EchA, epichlorohydrin epoxide hydrolase from *Agrobacterium radiobacter* AD1.

10.1021/bi9817257 CCC: $15.00
Published on Web 12/02/1998

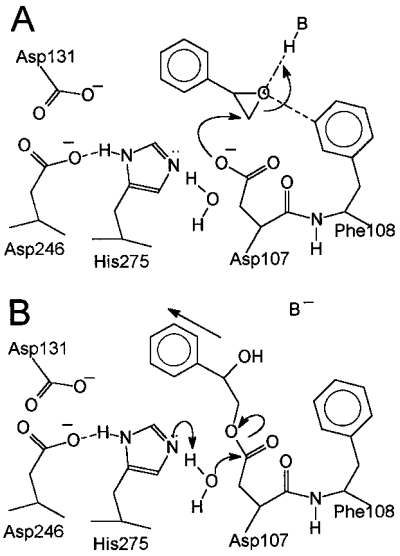

FIGURE 1: Proposed reaction mechanism for epoxide hydrolase. (A) Nucleophilic attack of Asp107 at the least-hindered carbon atom of styrene oxide, leading to the formation of a covalent ester intermediate. Presumably, an unidentified proton donor (B-H) assists in ring opening. (B) Proton abstraction from a water molecule by the His275-Asp246 pair, assisted by Asp131, and subsequent hydrolysis of the intermediate.

specific mutants, EchA was also classified as an α/β-hydrolase fold enzyme. It has a reaction mechanism in which Asp107 performs a nucleophilic attack on the primary carbon atom of the epoxide ring, leading to a covalently bound ester intermediate (Figure 1). The Asp246-His275 pair, supported by Asp131, then activates a water molecule that hydrolyzes the ester bond at the carbonyl function of Asp107, and product is released (*4*).

It turned out that EchA could discriminate between the enantiomers of styrene oxide and substituted variants thereof, affording the production of enantiomerically pure epoxides (*7*). Styrene oxide showed peculiar kinetics of conversion, since the (*R*)-enantiomer was completely hydrolyzed before the (*S*)-enantiomer, but the latter was subsequently converted at a much higher rate. How this sequential hydrolysis can be explained by reaction rates at the enzyme active site is the focus of this study.

To this end, we investigated the kinetics of styrene oxide conversion by means of steady-state and pre-steady-state kinetic experiments. Stopped-flow fluorescence and rapid-quench techniques were used to resolve the kinetic constants. The resulting kinetic constants could quantitatively describe the enantioselective conversion of racemic styrene oxide.

MATERIALS AND METHODS

Materials. (*R*)- and (*S*)-styrene oxide and (*R*)- and (*S*)-1-phenyl-1,2-ethanediol were purchased from Aldrich and were 97% enantiomerically pure as was confirmed by gas chromatographic analysis.

Protein Expression and Purification. *E. coli* BL21(DE3) with plasmid pEH20 containing the epichlorohydrin epoxide hydrolase gene *echA* of *A. radiobacter* AD1 under control of a T7 promoter was used for the expression of epoxide hydrolase. Protein was expressed and purified as described before (*4*). Enzyme was kept at 4 °C in PEMAG buffer (10 mM phosphate, pH 7.5, 1 mM EDTA, 1 mM β-mercaptoethanol, 0.02% sodium azide, and 10% (v/v) glycerol) and could be stored for over six months without losing activity.

Stopped-Flow Fluorescence. Stopped-flow fluorescence experiments were performed at 30 °C on an Applied Photophysics model SX.17MV apparatus. The tryptophan residues were excited at a wavelength of 290 nm, and the resulting fluorescence cut-off emission was recorded after passage through a 305 nm cutoff filter. Stock solutions of (*R*)- and (*S*)-styrene oxide were prepared in acetonitrile and were freshly diluted in TEMA buffer (50 mM Tris-SO_4, pH 9.0, 1 mM EDTA, 1 mM β-mercaptoethanol, and 0.02% sodium azide) to a final concentration of 0.5% (v/v) acetonitrile. Low concentrations of acetonitrile did not affect enzyme activity. Enzyme solutions were also prepared in TEMA buffer, and all mentioned concentrations are those after mixing. For single-turnover reactions the enzyme was concentrated in TEMA buffer by using an Amicon ultrafiltration cell with a PM-10 filter.

Rapid-Quench Experiments. Single-turnover experiments were performed at 30 °C on a RQF-63 rapid-quench-flow apparatus from Kintek Instruments. Concentrated enzyme and a freshly prepared styrene oxide solution from an acetonitrile stock were mixed, and the total volume of 100 μL was quenched with KOH to a final concentration of 0.7 M. The instability of styrene oxide under strongly basic conditions was overcome by directly injecting the quenched reaction mixture (217 μL) into a tube containing 61 μL of 2 M HCl, 200 μL of 1 M borate buffer, pH 9.0, and 0.5 mL of diethyl ether with 10 μM 1,9-dichlorononane as the internal standard. These quenching conditions could not prevent that a small fraction of the covalent ester intermediate was still hydrolyzed, but increasing the concentration of KOH or the use of HCl as a quenching agent resulted in nonenzymatic hydrolysis of styrene oxide.

Quantitative analysis of the styrene oxide in the ether phase was done by gas chromatography. The 1-phenyl-1,2-ethanediol that remained in the water phase was derivatized with 2,2-dimethoxypropane to give a hemiacetal that was easily detected by gas chromatography (*15*). For this procedure, 400 μL of the waterphase was saturated with sodium chloride and the diol was extracted with 0.6 mL of 2,2-dimethoxypropane with 10 μM 1,9-dichlorononane as the internal standard. The organic phase was then transferred to a sealed tube with 0.2 g of Amberlite IR-120 (H^+), a strongly acidic cation exchanger that is coated on polystyrene, and the derivatization reaction was completed by vigorous shaking at 30 °C for 1 h. Both the styrene oxide and the hemiacetal derivative of 1-phenyl-1,2-ethanediol were analyzed by gas chromatography using a 0.2 mm × 25 m CP-Wax-57CB column (Chrompack) and a flame-ionization detector.

Steady-State Parameters. The k_{cat} values of (*R*)- and (*S*)-styrene oxide were determined by following substrate depletion by gas chromatography. A vial with a sufficient amount of enzyme and 5 mM substrate was incubated at 30 °C, and at different times within 15 min samples of 1 mL were taken. The sample was extracted with 2 mL of diethyl ether with 10 μM 1,9-dichlorononane as the internal standard. The organic phase was analyzed on a 0.2 mm × 25 m CP-Wax-57CB column using a gas chromatograph equipped with a flame-ionization detector.

The K_m value for (*S*)-styrene oxide was determined by initial rate experiments. Sealed tubes with 10 mL of different substrate concentrations in TEMA buffer were incubated at 30 °C. At time zero an equal amount of enzyme was added to every tube. After 15 min of incubation, the reaction mixture was extracted with 1.5 mL of ice-cold diethyl ether with 10 μM 1,9-dichlorononane as the internal standard. The diol was derivatized and analyzed by gas chromatography as described above.

Data Analysis. The stopped-flow fluorescence and rapid-quench data were analyzed and fitted with the program MicroMath Scientist for Windows, version 2.0. The fluorescence traces (*F*) of the multiple-turnover experiments with (*R*)- and (*S*)-styrene oxide against time (*t*) were fitted to a double and a single exponential of the form $F = A1(e^{-k_{obs1}t}) + A2(e^{-k_{obs2}t}) + C$ and $F = Ae^{-k_{obs}t} + C$, respectively. The parameter *A* is the amplitude, k_{obs} is the observed rate constant, and *C* is the floating endpoint. The multiple-turnover traces for (*S*)-styrene oxide were corrected for 1.5% contamination with (*R*)-styrene oxide. Therefore, a fluorescence trace of (*R*)-styrene oxide that was simulated with the known enzyme and substrate concentrations together with the solved kinetic parameters and fluorescence factors was subtracted from the experimentally obtained multiple-turnover trace of (*S*)-styrene oxide, and the resulting trace was fitted to a single exponential. This simple correction method was a good approximation, since the affinity of epoxide hydrolase for (*R*)-styrene oxide was much higher than for (*S*)-styrene oxide. The conversion of (*R*)-styrene oxide was not influenced by the concentration of (*S*)-styrene oxide, but it was essential to keep the enzyme concentration higher than the concentration of the contaminating (*R*)-styrene oxide. Equations 5 and 7 for the multiple-turnover reactions with (*R*)- and (*S*)-styrene oxide, respectively, were directly fitted to the k_{obs} data to obtain a solution for the kinetic constants. The fit was constrained by the values of the steady-state parameters, which were allowed to vary within their margin of experimental error. The kinetic constants were refined by comparing fits of the single-turnover traces and the k_{obs} data.

To simulate the experimental fluorescence traces with the kinetic constants and the reaction schemes, we described the traces as the sum of the contributions of each enzyme species to the total fluorescence, that is, the relative concentration of each enzyme species multiplied by the corresponding fluorescence factor. The resulting relative fluorescence was multiplied by the experimentally observed fluorescence signal for free enzyme of that particular experiment.

Equations for k_{cat} and K_m were derived by using the determinant method (*16*). For (*R*)-styrene oxide the steady-state parameters were derived from Scheme 2 (eqs 1 and 2).

$$k_{cat} = \frac{k_2k_3k_4}{k_{-2}(k_{-3} + k_4) + k_2(k_3 + k_{-3} + k_4) + k_3k_4} \quad (1)$$

$$K_m = \frac{K_S(k_{-2}k_{-3} + k_{-2}k_4 + k_3k_4)}{k_{-2}(k_{-3} + k_4) + k_2(k_3 + k_{-3} + k_4) + k_3k_4} \quad (2)$$

The steady-state parameters for (*S*)-styrene oxide were derived from Scheme 3. The resulting equations could be simplified to eqs 3 and 4, since saturation of the k_{obs} could not be observed, meaning that Scheme 3 simplifies to a two-step mechanism in which the first step, the alkylation of the enzyme, is described with the parameters k_2/K_S and k_{-2}.

$$k_{cat} = k_3 \quad (3)$$

$$K_m = \frac{K_S(k_{-2} + k_3)}{k_2} \quad (4)$$

For simulations of single-turnover or multiple-turnover reactions with a given set of kinetic parameters, the initial enzyme concentration and the fluorescence factors were allowed to change within 5% in order to get the best fit to the experimental data.

Table 1: Steady-State Parameters of *A. radiobacter* AD1 Epoxide Hydrolase for the Conversion of (*R*)- and (*S*)-Styrene Oxide

substrate	K_m (μM)	k_{cat} (s^{-1})	k_{cat}/K_m (μM^{-1} s^{-1})
(*R*)-styrene oxide	0.6 ± 0.2[a]	4.2 ± 0.3	7 ± 1
(*S*)-styrene oxide	25 ± 5	10.5 ± 1	0.42 ± 0.2

[a] Calculated from $E = 16.2$.

RESULTS

Steady-State Kinetics of Styrene Oxide Conversion. The epoxide hydrolase of *A. radiobacter* AD1 (EchA) converts styrene oxide enantioselectively with an *E* value $((k_{cat,R}/K_{m,R})/(k_{cat,S}/K_{m,S}))$ of 16.2 (*7*). The k_{cat} and K_m of the enantiomers were separately determined in order to relate them to the observed enantioselectivity (Table 1). The k_{cat} values were determined by initial velocity measurements of substrate conversion by using gas chromatography. The K_m for (*S*)-styrene oxide could also be determined by initial rate measurements. The K_m for (*R*)-styrene oxide was too low to be directly determined by gas chromatography, but could be derived using the *E* value, and was calculated to be 0.6 μM (Table 1). The results show that the (*R*)-enantiomer, which is the worse substrate in terms of k_{cat}, is converted first because of its lower K_m value.

Significant product inhibition by (*R*)- and (*S*)-1-phenyl-1,2-ethanediol on the conversion of 1 mM (*R*)- or (*S*)-styrene oxide was not found at concentrations up to 50 mM, indicating that the product has a high dissociation constant. The amounts of product that were formed in the experiments that are described in this study were too low to be of mechanistic concern.

Single Turnover of Epoxide Hydrolase with (R)-Styrene Oxide. A single-turnover reaction with enzyme in excess over (*R*)-styrene oxide was monitored on a stopped-flow apparatus by following the intrinsic enzyme fluorescence in time (Figure 2A). The fluorescence trace clearly showed three distinct phases. Within the first 10 ms after mixing, the intrinsic enzyme fluorescence decreased rapidly after which the fluorescence signal increased to a maximum at 0.1 s and then decayed during 1.5 s until it reached the fluorescence of free enzyme again. Since three kinetic steps can be observed, a three-step mechanism is the minimal scheme needed to describe the data (Scheme 1). The contributions of the enzyme species ER-I and ER-II to the total fluorescence were unknown, and therefore, fitting of the single-turnover fluorescence trace resulted in multiple solutions of the kinetic constants that all agreed with the experimentally determined steady-state parameters of (*R*)-styrene oxide.

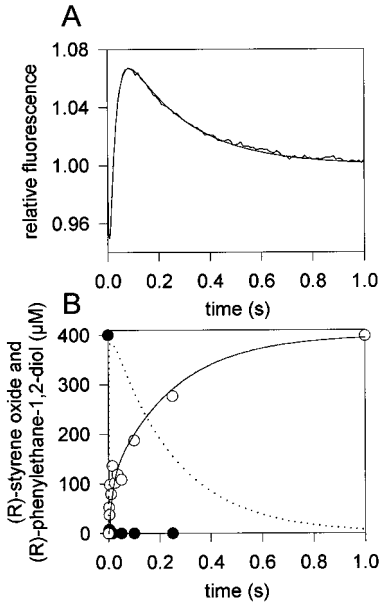

FIGURE 2: Single-turnover experiments with (*R*)-styrene oxide. (A) Stopped-flow fluorescence trace recorded with 18.7 μM enzyme and 12.5 μM (*R*)-styrene oxide at 30 °C. The solid line shows a simulation of the four-step model of Scheme 2 using the kinetic parameters of Table 2 and fluorescence factors for E-R and E-P of 0.85 and 1.1, respectively. (B) Rapid-quench experiment with 600 μM enzyme and 400 μM (*R*)-styrene oxide at 30 °C. Substrate (●) and product (○) concentrations were analyzed by gas chromatography. The solid lines represent simulations of substrate and product with the four-step mechanism of Scheme 2 and the data of Table 2. The dotted line represents the sum of the simulated covalent intermediates E-R and E-P.

Scheme 1

$$\text{E + R} \rightleftharpoons \text{ER-I} \rightleftharpoons \text{ER-II} \longrightarrow \text{E + P}$$

Scheme 2

$$\text{E + R} \underset{k_{-2}}{\overset{K_S}{\rightleftharpoons}} \text{ER} \underset{k_{-3}}{\overset{k_2}{\rightleftharpoons}} \text{E-R} \underset{}{\overset{k_3}{\rightleftharpoons}} \text{E-P} \xrightarrow{k_4} \text{E+P}$$

Although it seems likely that ER-I and ER-II represent the Michaelis complex and covalent intermediate, respectively, other possibilities cannot be excluded.

To find out the nature of species ER-I and ER-II, we performed a single-turnover experiment on a rapid-quench apparatus. The absolute concentrations of substrate and product at various times after mixing were measured (Figure 2B). The rapid-quench experiment showed fast disappearance of substrate within a few milliseconds after mixing and relatively slow formation of product. After 5 ms no substrate was left and almost no product had formed, meaning that a covalent intermediate had accumulated. This accumulation of intermediate coincided with the quenching of the fluorescence signal in Figure 2A. Thus, ER-I in Scheme 1 represents the covalent intermediate (E-R) and not the Michaelis complex (ER).

The slow appearance of product in the rapid-quench experiment suggests that the raise in fluorescence, corresponding to the formation of species ER-II in Scheme 1, was caused by a second covalent intermediate with different fluorescent properties. A steady-state fluorescence spectrum of free enzyme and enzyme with excess (*R*)-styrene oxide showed that the fluorescence increase is accompanied by a small red-shift of the fluorescence maximum from 326 to 331 nm.

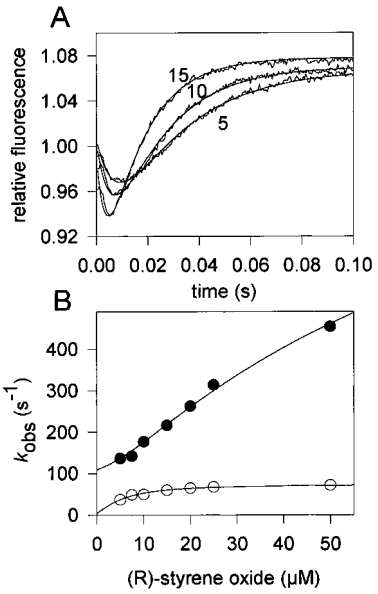

FIGURE 3: Multiple-turnover experiments with (*R*)-styrene oxide. (**A**) Fluorescence traces of 0.5 μM enzyme with 5, 10, and 15 μM (*R*)-styrene oxide at 30 °C. The solid line shows the fit of a two-exponential function to the data, leading to two k_{obs} values for each concentration. (B) Observed rate constants k_{obs1} (●) and k_{obs2} (○) plotted as a function of (*R*)-styrene oxide concentration. The solid curves show the fits of the analytical solutions of eq 5 and the kinetic parameters of Table 2 to the data.

To allow for a Michaelis complex and a second covalent intermediate the reaction of Scheme 1 has to be extended to a four-step mechanism (Scheme 2). Since the formation of the Michaelis complex (ER) appeared to be an extremely fast process, it is represented as a rapid equilibrium with a dissociation constant K_S. Species E-R and E-P represent kinetically observed distinct covalent states with different fluorescence properties. The single-turnover reactions that were done with stopped-flow and rapid-quench experiments did not provide sufficient information to yield a unique solution for the rate and equilibrium constants, and therefore, multiple-turnover experiments were performed.

Multiple-Turnover Reactions with (R)-Styrene Oxide. Multiple-turnover experiments were done with 0.5 μM epoxide hydrolase and 5−50 μM (*R*)-styrene oxide (Figure 3A). The fluorescence traces could be fitted with two exponential terms and yielded two rate constants (k_{obs1} and k_{obs2}) with opposite amplitudes. The k_{obs2} and to a lesser extend also k_{obs1} leveled off with increasing epoxide concentration. This indicates that not the Michaelis complex but a subsequent step, that is, the formation of the covalent intermediate (Figure 3B), caused the fluorescence quenching. In an experiment in which purified Asp107Ala mutant enzyme (*4*), which does not form a covalent intermediate, was mixed with 1 mM (*R*)-styrene oxide, no sign of quenching of the intrinsic protein fluorescence could be observed, further indicating that enzyme-bound substrate does not influence the fluorescence signal.

At substrate concentrations higher than 50 μM, k_{obs1} could not be determined accurately, since the fluorescence decrease occurred largely in the dead time of the instrument (1.5 ms). At substrate concentrations above 400 μM, the visible part of this first exponential decrease seemed to remain un-

Table 2: Kinetic Constants for Epoxide Hydrolase Determined at 30 °C and pH 9.0

	kinetic constants							steady-state constants		
substrate	K_S (μM^{-1})	k_2 (s^{-1})	k_2/K_S (μM^{-1} s^{-1})	k_{-2} (s^{-1})	k_3 (s^{-1})	k_{-3} (s^{-1})	k_4 (s^{-1})	k_{cat} (s^{-1})	K_m (μM)	k_{cat}/K_m (μM^{-1} s^{-1})
(*R*)-styrene oxide	90 ± 10	1100 ± 100	12.2 ± 1	40 ± 5	70 ± 5	<4	4.2 ± 0.2	3.8	0.46	8.3
(*S*)-styrene oxide	>500	>400	0.72 ± 0.06	4 ± 2	10.5 ± 0.2			10.5	21	0.5

Scheme 3

$$E + S \underset{}{\overset{K_S}{\rightleftharpoons}} ES \underset{k_{-2}}{\overset{k_2}{\rightleftharpoons}} E\text{-}S \xrightarrow{k_3} E + P$$

changed, indicating that at these concentrations the Michaelis complex is saturated. The second rate constant, k_{obs2}, which corresponds to the transient raise in fluorescence, showed a hyperbolic dependence on substrate concentration and did not change significantly at concentrations above 50 μM, indicating that this reaction step already saturates at low substrate concentrations.

To obtain an analytical solution for k_{obs1} and k_{obs2}, we assumed that Scheme 2 approximates a sequence of first-order reactions when (*R*)-styrene oxide is at least in 10-fold excess over enzyme. The solutions for k_{obs1} and k_{obs2} were obtained by following the procedure described by Cornish-Bowden (*17*):

$$k_{obs1,2} = 0.5P \pm 0.5\sqrt{P^2 - 4Q}$$

$$P = k_2\frac{[R]}{K_S + [R]} + k_{-2} + k_3 + k_{-3} + k_4 \qquad (5)$$

$$Q = k_2(k_3 + k_{-3} + k_4)\frac{[R]}{K_S + [R]} + k_{-2}(k_{-3} + k_4) + k_3k_4$$

These equations were used to fit the data of k_{obs1} and k_{obs2} and resulted in unique values for all the kinetic parameters (Table 2). The steady-state parameters for (*R*)-styrene oxide (Table 1) were used as a constraint during the fitting procedure in the form of eq 1 and 2, and they were allowed to vary within their margin of error. The restriction of the fit by steady-state parameters was necessary to get a solution for k_4, which otherwise would approach 0. The value for k_{-3} could not be determined exactly. It could be varied between 0 and 4 s^{-1} without severely disturbing the fit, as long as the value for k_{-3} did not exceed the value for k_4. We could not conclude if the third step of Scheme 3 was either irreversible or slightly reversible.

The derived kinetic constants from the multiple-turnover experiment were used to simulate the single-turnover reactions that were done by stopped-flow fluorescence and by rapid-quench (Figure 2). The stopped-flow fluorescence trace was fitted by using the fluorescence factors for the enzyme species as the only variables, resulting in fluorescence factors for E-R and E-P of 0.85 and 1.1, respectively. The fluorescence factor of the Michaelis complex ER was set to 1, since no quenching of the intrinsic protein fluorescence was observed for this enzyme species. The substrate depletion curve of the rapid-quench experiment, which was not used as a restraint in the fitting procedures, could be simulated well (Figure 2B). The experiment showed some rapid formation of product in the early stage of the single-turnover reaction, which was caused by slight instability of the covalent intermediate during quenching. Assuming that 20% of the ester intermediate is being hydrolyzed during quenching, progress of product formation was well predicted with the kinetic constants given in Table 2. The possibility that enzyme species E-P represents an enzyme-bound product instead of a covalent intermediate could be eliminated, since simulations showed that product formation in the rapid-quench experiment was too slow for this alternative.

Conformational Change Prior to Substrate Binding. When multiple-turnover experiments were performed by stopped-flow fluorescence with (*R*)-styrene oxide concentrations of 50 μM and higher, an extra exponential raise was visible after the initial exponential raise (k_{obs2}). This exponential had a low rate constant (1−3 s^{-1}) and had an amplitude that was at least 30 times smaller than the amplitude for k_{obs2}. This additional small exponential cannot be caused by the last reaction step (4.2 s^{-1}), since each kinetic constant along the pathway should be higher than k_{cat} (*18*). The only plausible explanation is that it is due to an enzyme isomerization prior to substrate binding (*18*). Simulations indicated that less than 5% of the enzyme was in a state that needed a slow conformational change before substrate binding. The effect of this is too small to influence the kinetic constants obtained in single-turnover and multiple-turnover experiments.

Kinetics of (S)-Styrene Oxide Conversion. Single-turnover reactions with (*S*)-styrene oxide were done by stopped-flow fluorescence and by rapid-quench techniques (Figure 4). The fluorescence trace from the single-turnover reaction with (*S*)-styrene oxide (Figure 4A) was clearly different from the trace obtained with (*R*)-styrene oxide (Figure 2A), since no transient increase in the fluorescence signal could be observed with the (*S*)-enantiomer. The single-turnover trace of (*S*)-styrene oxide showed only two phases, a fast phase with a decrease of fluorescence and a subsequent slower recovery of the enzyme fluorescence. The rapid-quench data showed that, with (*S*)-styrene oxide, most of the covalent intermediate is formed within the first 50 ms, indicating that the quenching of the intrinsic protein fluorescence was caused by the formation of covalent intermediate (Figure 4B). Mixing of the Asp107Ala mutant enzyme with 1 mM (*S*)-styrene oxide did not result in any change of the intrinsic protein fluorescence, indicating that formation of the Michaelis complex did not affect the fluorescence signal. The minimal mechanism needed to describe the data contains three reaction steps (Scheme 3).

Fitting of the single-turnover fluorescence traces with steady-state restrictions given by eqs 3 and 4 only yielded a unique solution for the kinetic parameters when the formation of the covalent intermediate (E−S) in Scheme 3 from free enzyme and substrate (E + S) via the Michaelis complex (ES) was taken as a single kinetic step, resulting in values for k_2/K_S, k_{-2}, and k_3. No unique solution for K_S and k_2 could be obtained from single-turnover reactions.

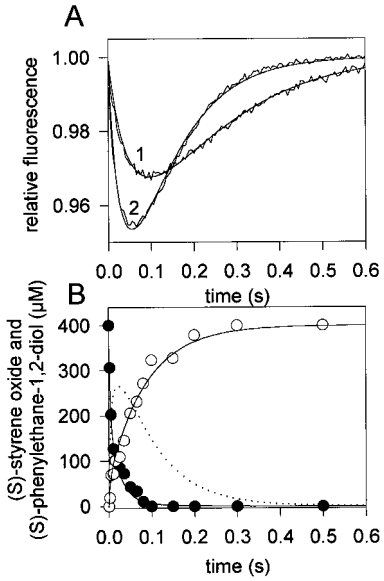

FIGURE 4: Single-turnover experiments with (*S*)-styrene oxide. (A) Stopped-flow fluorescence traces of 18.7 μM enzyme and 12.5 μM substrate (1) and 44 μM enzyme and 35 μM substrate (2). The solid lines show a fit of the data by the three-step mechanism of Scheme 3 and the data of Table 2, using a fluorescence factor of 0.85 for the covalent intermediate. (B) Rapid-quench experiment, using 335 μM enzyme and 400 μM substrate. Substrate (●) and product (○) concentrations were determined by gas chromatography. The solid lines show simulations of the substrate and product concentrations with the three-step model of Scheme 3 and the data of Table 2. The dotted line shows the simulated concentrations of covalent intermediate during turnover.

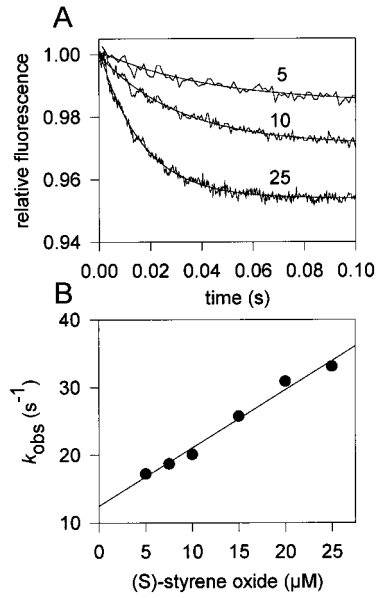

FIGURE 5: Multiple-turnover experiments with (*S*)-styrene oxide. (A) Fluorescence traces of 0.5 μM enzyme with 5, 10, and 25 μM (*S*)-styrene oxide at 30 °C. The data were fitted with a single exponential, yielding a rate constant for each concentration. (B) Observed rate constants (k_{obs}) as a function of the concentration of (*S*)-styrene oxide. Data were obtained from multiple-turnover curves as described in Materials and Methods. The solid line is a fit of eq 7 and the kinetic parameters of Table 2 to the data.

Multiple-turnover experiments were done with 0.5 μM epoxide hydrolase and 5−25 μM (*S*)-styrene oxide in order to obtain more restraints (Figure 5A). These reactions could only be performed at low substrate concentrations, since commercially available (*S*)-styrene oxide was contaminated with 1.5% (*R*)-styrene oxide, which interfered too much with the fluorescence signal when the concentration of the (*R*)-enantiomer approximated the concentration of enzyme. To obtain better data, even at low substrate concentrations, the multiple-turnover fluorescence traces of (*S*)-styrene oxide were corrected for (*R*)-styrene oxide contamination before the traces were fitted to a single exponential (Material and Methods). This simplified correction was allowed, since the affinity of epoxide hydrolase for the (*R*)-enantiomer was far higher than for the (*S*)-enantiomer, resulting in a (*S*)-enantiomer concentration-independent conversion of the contaminating fraction of (*R*)-styrene oxide. The experimental traces that were fitted in this way resulted in single exponentials (k_{obs}) that were linearly dependent on substrate concentration (Figure 5B). Since the multiple-turnover reactions were done under pseudo-first-order conditions, exact solutions for k_{obs} in terms of the rate constants were derived from Scheme 3 (eqs 6 and 7).

$$k_{obs} = \frac{k_2[S]}{[S] + K_S} + k_{-2} + k_3 \quad (6)$$

$$k_{obs} = \frac{k_2}{K_S}[S] + k_{-2} + k_3 \quad (7)$$

The formula of eq 6, which shows the concentration dependency of k_{obs}, corresponds to a hyperbola with an intercept at the *y*-axis of $k_{-2} + k_3$. The experimental data showed no sign of saturation, indicating a high K_S. Therefore, the function for k_{obs} can be simplified to eq 7. The k_{obs} data of Figure 5 were fitted simultaneously with the single-turnover traces and the fits were restricted by the steady-state parameters (Table 1) that are given by eqs 3 and 4. Only the ratio k_2/K_S could be determined, and therefore, only lower limits could be set for k_2 and K_S (Table 2). Unique solutions could be found for k_{-2} and for the rate-limiting step k_3. Almost identical values for the kinetic constants were obtained from the multiple-turnover experiments and the single-turnover reactions, and the solution of the combined fit of both experiments is shown in Table 2.

Kinetics of Racemic Styrene Oxide Conversion. The kinetic mechanism and associated parameters derived for the separate enantiomers of styrene oxide should explain the enantioselective hydrolysis of racemic styrene oxide. The sequential conversion of racemic styrene oxide by epoxide hydrolase could be followed by stopped-flow fluorescence signals, since the fluorescence of the enzyme was elevated and decreased during the steady-state conversion of (*R*)- and (*S*)-styrene oxide, respectively (Figure 6A). With the determined kinetic constants and the derived fluorescence factors it was possible to simulate the fluorescence trace (Figure 6A) and the substrate depletion curve as determined by chiral gas chromatography (Figure 6B). From the calculated k_{cat} and K_m for both enantiomers (Table 2) an *E* value of 16.6 was calculated, which is in close agreement with the *E*-value of 16.2 that was determined from kinetic resolution experiments (*7*).

DISCUSSION

Overall Kinetic Mechanism. This study describes the kinetic mechanism of the epoxide hydrolase (EchA) from

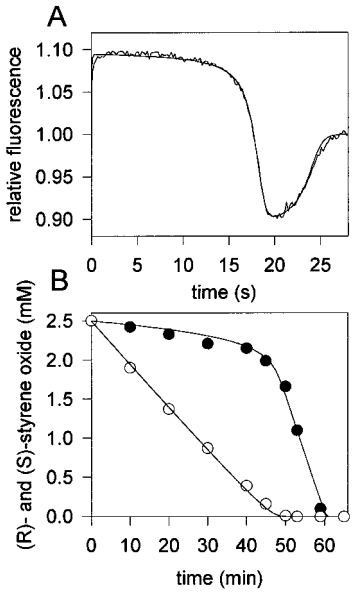

FIGURE 6: Multiple-turnover experiment with racemic styrene oxide. (A) Fluorescence trace recorded with 3.5 μM enzyme and 500 μM styrene oxide at 30 °C. The solid line shows a simulation with Schemes 2 and 3 and the data of Table 2. (B) Kinetic resolution of 5 mM styrene oxide with 15 μM enzyme. Data were taken from Lutje Spelberg et al. (*7*), and they show the degradation of (*R*)-styrene oxide (○) and (*S*)-styrene oxide (●) in time. The fits were obtained by using the formulas for competitive Michaelis−Menten kinetics combined with first-order chemical hydrolysis of the substrate as described by Lutje Spelberg et al. (*7*) with the steady-state parameters described in Table 2.

Agrobacterium radiobacter AD1. The conversion of both enantiomers of styrene oxide is described in terms of equilibrium and reaction rate constants which were solved using stopped-flow fluorescence and rapid-quench techniques. These experiments were possible since the reaction proceeds regiospecifically by exclusive attack of the nucleophilic Asp107 at the primary carbon atom of styrene oxide, which was demonstrated by the observation that the stereochemical configuration of the substrate was retained in the product (*7*). The incorporation of ^{18}O-labeled water into epichlorohydrin by *A. radiobacter* AD1 epoxide hydrolase also occurred solely at the least-hindered carbon atom (14).

A striking difference between the reaction schemes that describe the conversion of both enantiomers of styrene oxide was the number of reaction steps. At least three kinetic steps are needed to describe a kinetic mechanism of an enzyme reaction that involves a Michaelis complex, the formation of a covalent intermediate, and its hydrolysis to product. The conversion of (*S*)-styrene oxide could well be described by such a three-step mechanism, but for (*R*)-styrene oxide an additional kinetic step was observed. This appeared to be a unimolecular isomerization preceding the hydrolysis of the covalent intermediate, leading to a four-step mechanism. Despite the difference in the number of kinetic steps, the kinetics of the conversion of the enantiomers share common characteristics.

Fast substrate binding followed by rapid and reversible alkylation of the enzyme was observed for both enantiomers of styrene oxide. With (*R*)-styrene oxide, the alkylation rate (1100 s^{-1}) is very fast compared to the dealkylation rate (40 s^{-1}), and the same was found for the conversion of (*S*)-styrene oxide for which the alkylation rate (>400 s^{-1}) was at least 2 orders of magnitude higher than the dealkylation rate (4 s^{-1}). The reaction step after the formation of the covalent intermediate (k_3), that is, hydrolysis of the alkyl-enzyme in case of (*S*)-styrene oxide and a unimolecular isomerization step in case of (*R*)-styrene oxide, is about twice as fast as the dealkylation rate ($k_{-2} < k_3$) for both enantiomers, meaning that the alkyl-enzymes only have a slight preference for the forward reaction. The second covalent state in the reaction pathway of (*R*)-styrene oxide, which is formed after the unimolecular isomerization, is a more stable enzyme species than the first covalent state, due to the low value of k_{-3}. The kinetic mechanism of the conversion of (*R*)- and (*S*)-glycidyl-4-nitrobenzoate by rat microsomal epoxide hydrolase also shows a fast and reversible alkylation of the enzyme, but the dealkylation rates are faster than the hydrolysis rates ($k_{-2} > k_3$) (*8*). The possibility of a conformational change was considered for the conversion of glycidyl-4-nitrobenzoate by rat microsomal epoxide hydrolase, but it was judged unlikely since this extra step did not fit the kinetic data (*10*).

The rate-limiting step for the conversion of both enantiomers of styrene oxide by EchA is the hydrolysis of the covalent intermediate, which has a rate constant approximately equal to the overall k_{cat}. Since the alkylation rate of the enzyme is much higher than the hydrolysis rate for both isomers, the covalent intermediate extensively accumulated during turnover. This accumulation of alkylated enzyme is the reason that the K_m values for the (*R*)- and (*S*)-enantiomers (0.46 and 21 μM) were about 20−200-fold lower than the substrate-binding constant K_S (90 and >400 μM). Rate-limiting hydrolysis of the alkyl-enzyme and its accumulation during steady-state turnover was also found for rat microsomal epoxide hydrolase (*8*−*10*).

The reversibility of the formation of the covalent intermediate may also explain that a previously described His275Arg mutant of EchA, that could only efficiently perform the alkylation reaction with epichlorohydrin but not the hydrolysis reaction, showed incomplete conversion of substrate when excess enzyme was added (*4*). Thus, reversible alkylation caused only 50−70% of substrate to be covalently captured by the mutant enzyme, while the rest stayed in the form of a Michaelis complex or a free substrate. A His275Gln mutant did not show accumulation of covalent intermediate, although it could hydrolyze epichlorohydrin to the same extent as the His275Arg EchA (<0.001 s^{-1}) (*4*), indicating that the alkylation rate of this mutant enzyme was low compared to the dealkylation and the hydrolysis rates.

The Unimolecular Isomerization during Conversion of (R)-Styrene Oxide. During the conversion of (*R*)-styrene oxide a unimolecular isomerization of the covalent enzyme−substrate complex was observed before hydrolysis took place. This isomerization step is relatively fast compared to the hydrolysis rate (70 vs 4.2 s^{-1}), and therefore, the enzyme accumulated predominantly in this second covalent state during steady-state turnover. This enzyme species was easily detectable due to enhancement of the intrinsic protein fluorescence, whereas the first covalent intermediate (E-R in Scheme 2) had a lowered fluorescence signal. The unimolecular isomerization step may be slightly reversible, but the back-rate is lower than 4 s^{-1}. An isomerization step was not observed with (*S*)-styrene oxide.

The tryptophan fluorescence maximum of free EchA is rather low (326 nm) compared to the fluorescence maximum of the unfolded state (350 nm), indicating that the tryptophan residues are packed in a hydrophobic surrounding. The isomerization step is accompanied by an increase of total fluorescence and a red-shift of the fluorescence maximum of about 5 nm, indicating that one or more of the tryptophan residues becomes close to a charged group or becomes exposed to water (*19*). On the basis of the catalytic mechanism three possible steps that lead to this change in fluorescence may be considered: protonation of the oxirane oxygen or some residue after ring cleavage (alkylation); a conformational change that is required for hydrolysis; or an intramolecular rearrangement due to acyl transfer.

Proton transfer rates are usually fast and do not influence enzyme kinetics, but in some cases proton transfer may be involved in slow steps, such as conformational changes (*20*). In principle, the protonation of the oxyanion that is formed upon opening of the oxirane ring could be a separate kinetic step, which may be rather slow during the conversion of (*R*)-styrene oxide. More likely, the isomerization step is a conformational change that allows a group nearby a tryptophan residue to be protonated or deprotonated, thereby increasing the total fluorescence signal of the enzyme. Enhancement of intrinsic protein fluorescence due to changes in pH of the surrounding buffer and uptake of a proton by the enzyme during substrate binding has been described (*21*, *22*). Due to the protonation of a carboxylate group during a rearrangement step of lysozyme-bound saccharide, the fluorescence signal of a nearby tryptophan was enhanced (*22*). In calsequistrin, the binding of a calcium ion or a proton caused a conformational change that externalizes a buried tryptophan, again resulting in an enhancement of the intrinsic protein fluorescence (*21*). These examples indicate that the fluorescence enhancement during the turnover of (*R*)-styrene oxide by epoxide hydrolase could be caused by electrostatic or conformational changes during reprotonation of the group that protonates the oxirane oxygen during ring opening.

An alternative explanation is that the kinetically observed isomerization step in the alkyl-enzyme involves repositioning of the bound substrate in the active site to make it susceptible for hydrolysis. In the first half reaction, the carboxylate anion of Asp107 must act as a nucleophile. In the second, the carbonyl function of the ester bond acts as an electrophilic center, presumably with the assistance of hydrogen-bonding interactions from the oxyanion hole. These same interactions would lead to a less reactive carboxylate in the alkylation step. Thus, a conformational readjustment of the ester intermediate may be needed for hydrolysis by a His275-activated water molecule in case of (*R*)-styrene oxide. This conformational change may cause a change in fluorescence with (*R*)-styrene oxide if the interaction between the aromatic ring of the substrate and a tryptophan in the active site is altered.

Finally, the isomerization may be a chemical step, that is, an acyl group migration which involves nucleophilic attack of the C_2 hydroxyl group of the covalently bound substrate on the carbonyl function of Asp107, leading to a different covalent intermediate which may be more susceptible to hydrolysis. In aqueous solutions, the transfer rates of acyl groups are on the order of 10^{-3} s^{-1} (*9*), but this step may be much faster in the active site of an enzyme. The possibility of acyl group migration was considered by Tzeng et al. (*9*) to explain the kinetics of the Glu404Gln mutant of rat microsomal epoxide hydrolase. They argue that a dead-end complex that is formed during the conversion of glycidyl-4-nitrobenzoate fits with the observed kinetics of this mutant and that reversible enzymic acyl transfer might cause such a complex (*9*). For discrimination between the various options for the isomerization steps, further characterization of the accumulating covalent intermediate by spectroscopic or chemical methods is needed.

The Role of Tryptophans in Substrate Binding. The observed changes in the intrinsic protein fluorescence during the turnover of styrene oxide indicate that one or more tryptophan residues are located near the active site. EchA has a total of eight tryptophan residues, but a survey of the secondary structure (*4*) and the three-dimensional structure of haloalkane dehalogenase (*23*), which has sequence similarity with epoxide hydrolase, only leaves the tryptophan residues 38, 151, and 183 as candidates. The intrinsic protein fluorescence decreases about 15% during alkylation of the enzyme, suggesting that only one tryptophan is completely quenched. Tryptophan 38 is part of the oxyanion hole sequence HGWP which is completely conserved among the microsomal and bacterial epoxide hydrolases and present as HGFP among the soluble epoxide hydrolases (*1*, *2*, *4*). The backbone amide of Trp38 in the oxyanion hole stabilizes the oxyanion formed on the nucleophilic Asp107 during hydrolysis of the ester bond, meaning that this residue is located close to the active site (*1*, *4*). Tzeng et al. (*9*) replaced the analogous Trp150 residue of microsomal epoxide hydrolase by phenylalanine and found less quenching of the intrinsic protein fluorescence during turnover and a 10-fold reduction of the k_{cat}. Preliminary results of the Trp38Phe mutant of EchA showed a 100-fold reduction in k_{cat} and no quenching of the intrinsic protein fluorescence during turnover, indicating that Trp38 is important for stabilization of the oxyanion during hydrolysis and that it may possibly play a role in substrate binding (R. Rink, unpublished results). Trp151 and Trp183 also have to be considered for a role in substrate binding, since they are situated in the cap domain of epoxide hydrolase. In haloalkane dehalogenase, tryptophan 175, which is located in the cap domain, is involved in substrate binding (*24*, *25*).

The Enantioselectivity of Epoxide Hydrolase. The kinetic mechanisms of *A. radiobacter* epoxide hydrolase and rat microsomal epoxide hydrolase are similar, but the enantioselectivity is governed by different factors. In rat microsomal epoxide hydrolase, the enantioselectivity for (*R*/*S*)-glycidyl-4-nitrobenzoate is most pronounced in the rate-limiting hydrolysis of the ester intermediate, since the faster hydrolyzed (*R*)-enantiomer is converted before the (*S*)-enantiomer, which is hydrolyzed 10 times slower (*8*). This is not the case for the conversion of (*R*/*S*)-styrene oxide by EchA, since the faster converted (*S*)-enantiomer is hydrolyzed after the (*R*)-enantiomer. This sequential hydrolysis of a racemate in which the second enantiomer is hydrolyzed faster has also been observed for the hydrolysis of styrene oxide and *tert*-butyloxirane by microsomal epoxide hydrolase (*26*, *27*). There was no mention of kinetic parameters in these studies, but the observed enantioselectivity suggests that microsomal epoxide hydrolase also has much lower k_{cat} and K_m values for the enantiomer which is converted first.

$$E = \frac{\left(\frac{k_{cat}}{K_m}\right)_R}{\left(\frac{k_{cat}}{K_m}\right)_R} = \frac{\left(\frac{k_2}{K_S}\right)_R}{\left(\frac{k_2}{K_S}\right)_S} \frac{\left(\frac{k_3 k_4}{k_{-2}k_{-3} + k_{-2}k_4 + k_3 k_4}\right)_R}{\left(\frac{k_3}{k_{-2} + k_3}\right)_S} \quad (8)$$

The enantioselectivity of epoxide hydrolase for racemic styrene oxide is totally caused by the ratio of the K_m values for the enantiomers, which is about 46. In fact, the ratio of the k_{cat} values reduces the enantioselectivity to 16.6. Equation 8 shows the E value as a function of the ratio of the alkylation rates for both enantiomers (k_2/K_S) and the remaining kinetic constants. Filling in the values for the kinetic constants from Table 2 shows that the E value is largely dictated by the difference in alkylation rates since the second terms with the remaining kinetic constants cancel each other. The differences in the dealkylation rates would annihilate the enantioselectivity caused by differences in alkylation efficiencies, if there were no extra unimolecular conformational change in the kinetic mechanism of (*R*)-styrene oxide that leads to increased capturing of the substrate.

REFERENCES

1. Arand, M., Grant, D. F., Beetham, J. K., Friedberg, T., Oesch, F., and Hammock, B. D. (1994) *FEBS Lett. 338*, 251−256.
2. Beetham, J. K., Grant, D., Arand, M., Garbarino, J., Kiyosue, T., Pinot, F., Oesch, F., Belknap, W. R., Shinozaki, K., and Hammock, B. D. (1995) *DNA Cell Biol. 14*, 61−71.
3. Misawa, E., Chan Kwo Chion, C. K. C., Archer, I. V., Woodland, M. P., Zhou, N-.Y., Carter, S. F., Widdowson, D. A., and Leak, D. J. (1998) *Eur. J. Biochem. 253*, 173−183.
4. Rink, R., Fennema, M., Smids, M., Dehmel, U., and Janssen, D. B. (1997) *J. Biol. Chem. 272*, 14650−14657.
5. Archer, I. V. J. (1997) *Tetrahedron 53*, 15617−15662.
6. Archelas, A., and Furstoss, R. (1998) *Trends Biotechnol. 16*, 108−116.
7. Lutje Spelberg, J. H., Rink, R., Kellogg, R. M., and Janssen, D. B. (1998) *Tetrahedron: Asymmetry 9*, 459−482.
8. Tzeng, H.-F., Laughlin, L. T., Lin, S., and Armstrong, R. M. (1996) *J. Am. Chem. Soc. 118*, 9436−9437.
9. Tzeng, H.-F., Laughlin, L. T., and Armstrong, R. M. (1998) *Biochemistry 37*, 2905−2911.
10. Laughlin, L. T., Tzeng, H.-F., Lin, S., and Armstrong, R. N. (1998) *Biochemistry 37*, 2897−2904.
11. Ollis, D. L., Cheah, E., Cygler, M., Dijkstra, B., Frolow, F., Franken, S. M., Harel, M., Remington, S. J., Silman, I., Schrag, J., Sussman, J. L., Verschueren, K. H. G., and Goldman, A. (1992) *Protein Eng. 5*, 197−211.
12. Koonin, E. V., and Tatusov, R. L. (1994) *J. Mol. Biol. 244*, 125−132.
13. von Dippe, P., Amoui, M., Alves, C., and Levy, D. (1993) *Am. J. Physiol. 264*, G528-G534.
14. Jacobs, M. H. J., van den Wijngaard, A. J., Pentenga, M., and Janssen, D. B. (1991) *Eur. J. Biochem. 202*, 1217−1222.
15. Weijers, C. A. G. M. (1997) *Tetrahedron: Asymmetry 8*, 639−647.
16. Huang, C. Y. (1979) *Methods Enzymol. 63*, 54−84.
17. Cornish-Bowden, A. (1995) *Fundamentals of Enzyme Kinetics*, Portland Press Ltd, London, U.K.
18. Johnson, K. A. (1992) *The Enzymes 20*, 1−61.
19. Creighton, T. E. (1989) *Protein Structure; A Practical Approach*, Oxford University Press, Oxford, U.K.
20. Gutfreund, H. (1995) *Kinetics for the Life Sciences: Reporters, Transmitters and Catalysts*, Cambridge University Press, Cambridge, U.K.
21. Hildago, C., Donoso, P., and Rodriguez, H. (1996) *Biophys. J. 71*, 2130−2137.
22. Halford, S. E. (1975) *Biochem. J. 149*, 411−422.
23. Verschueren, K. H. G., Franken, S. M., Rozeboom, H. J., Kalk, K. H., and Dijkstra, B. W. (1993) *J. Mol. Biol. 232*, 856−872.
24. Kennes, C., Pries, F., Krooshof, G. H., Bokma, E., Kingma, J., and Janssen, D. B. (1995) *Eur. J. Biochem. 228*, 403−407.
25. Verschueren, K. H. G., Seljeé, F., Rozeboom, H. J., Kalk, K. H., and Dijkstra, B. W. (1993) *Nature 363*, 693−698.
26. Watabe, T., Ozawe, N., and Hiratsuka, A. (1981) *Biochem. Pharmacol. 30*, 1695−1698.
27. Wistuba, D., and Schurig, V. (1992) *Chirality 4*, 178−184.

BI9817257